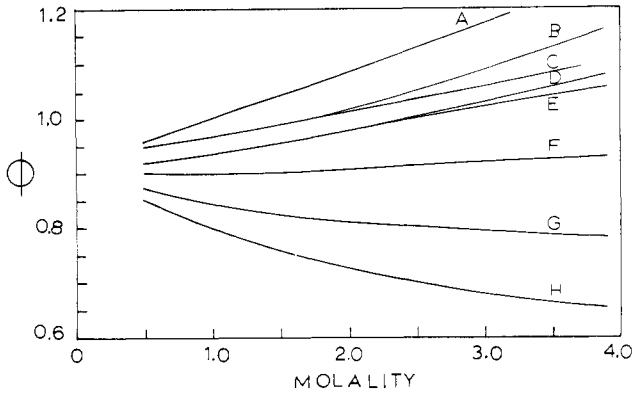

Figure 1. Osmotic coefficients of sulfamate and methanesulfonate salts: (A) lithium methanesulfonate, (B) tetramethylguanidinium methanesulfonate, (C) lithium sulfamate, (D) tetramethylguanidinium sulfamate, (E) sodium methanesulfonate, (F) potassium methanesulfonate, (G) sodium sulfamate, (H) potassium sulfamate. These are plotted from smoothed data.

A comparison of the osmotic coefficients of the sulfamate and methanesulfonate salts is shown graphically in Figure 1. The coefficients of the methanesulfonate salts are larger than those of the corresponding sulfamate salts for all cations. The differences for the lithium and tetramethylguanidinium salts are not as large, however, as for the sodium and potassium salts. It would be expected that the two former cations would ion pair with either anion to a greater extent than the sodium or potassium ion. Any cation ion pairing with the sulfamate anion would be at the expense of the anion ion pairing which has been postulated, and should reduce the difference in the values of the coefficients of the sulfamate and methanesulfonate salts. Alternatively, if the difference in the coefficients is due, in part, to a difference in the solvent structure altering properties of the sulfamate and methanesulfonate anions, the cation–anion pairing should also reduce this effect.

Registry No. Lithium sulfonate, 84849-43-4; tetramethylguanidinium sulfonate, 84849-44-5.

Literature Cited

(1) Bonner, O. D. *J. Chem. Eng. Data* **1982**, *27*, 143.
(2) Bonner, O. D. *J. Chem. Thermodn.* **1979**, *11*, 559.
(3) Robinson, R. A.; Sinclair, D. A. *J. Am. Chem. Soc.* **1934**, *56*, 1830.

Received for review August 23, 1982. Accepted January 7, 1983.

Thermophysical Properties of Ethylene in the Critical Region

Mohammed S. Nehzat, Kenneth R. Hall, and Philip T. Eubank*

Department of Chemical Engineering, Texas A&M University, College Station, Texas 77843

Thermophysical properties for ethylene were correlated in the critical region of 280.15–284.15 K, 4.5–11.0 mol/dm³ based on the experimental density measurements of Douslin and Harrison. Extrapolations of the measurements to the critical point (CP) are consistent with modern knowledge of critical-region behavior; the present tables agree with the derived thermodynamic properties of Harrison and Douslin at the above boundaries and, hence, form critical-region companion tables to those of Harrison and Douslin which are further from the CP. In addition to density, enthalpy, and entropy, the isochoric heat capacity is reported in both the homogeneous and heterogeneous regions with sonic velocities also tabulated along the homogeneous side of the saturation envelope.

Ethylene, the leading petrochemical, is frequently pumped across international boundaries and through common carrier pipelines where the volume of the fluid read from flowmeters must be converted to mass from *accurate* knowledge of the density. Metering conditions are often close to the critical point of 282.3502 K (~48.6 °F) and 5.04197 MPa (~730 psia). Discrepancies in the third significant figure of density have led to legal disputes involving millions of dollars per annum in separate cases. The high sensitivity of density to pressure and temperature in the critical region creates problems for single plant inventories as well as the simultaneous use of one pipeline by several firms. The objective of the present work is to provide derived thermophysical properties for ethylene on a fine grid pattern in the immediate critical region.

The present work was completed in 1978; we acknowledge that a number of technical articles concerning ethylene have been published since that time which are uncited and not used in the present correlation.

Critical Constants

The critical temperature was determined by fitting the orthobaric densities of Douslin and Harrison (*1*) to

$$\rho_l - \rho_g = a_1[1 - T/a_2]^{a_3} \quad (1)$$

where a_2, the critical temperature, was found to be 282.3502 ± 0.0105 K (IPTS – 68), ±0.01 K is attributed to experimental error, and ±0.0005 K is twice the standard deviation of eq 1 to fit the experimental data. The critical density was then found from extrapolation of the rectilinear diameter line to the critical temperature. Finally, the critical pressure was obtained from a nonanalytical vapor pressure equation considered below. The differences between the critical constants selected by Douslin and Harrison and those determined as above were within the precision of the experimental measurements as also noted by Harrison and Douslin (*2*). Thus, the following values of Douslin and Harrison were adopted: T_c = 282.3502 ± 0.0105 K, P_c = 5.04197 ± 0.0026 MPa, and ρ_c = 7.635 ± 0.006 mol/dm³. For ρ_c, we judge ±0.004 mol/dm³ to come from experiment and ±0.002 mol/dm³ from the fitting procedure. For P_c, ±0.0014 MPa is from the fitting procedure whereas ±0.0012 is estimated from experiment. These constants are in good agreement with Moldover's (*3*) visual observations, T_c = 282.344 ± 0.004 K and ρ_c = 7.650 ± 0.021 mol/cm³, but they are considerably lower than those adopted by Angus et al. (*4*): T_c = 282.65 ± 0.25 K, P_c = 5.076 ± 0.020 MPa, and ρ_c = 7.771 ± 0.071 mol/dm³. Recently, Hastings et al. (*5*) have selected T_c = 282.3452 ± 0.0017 K, P_c = 5.0403 ± 0.0002

0021-9568/83/1728-0205$01.50/0

Table I. Saturated Properties of Ethylene in the Critical Region

		ρ/(mol/dm^3)		U/(J/mol)			H/(J/mol)			S/(J/(mol K))		
T_{68}, K	P, MPa	ρ_l	ρ_g	U_l	ΔU_v	U_g	H_l	ΔH_v	H_g	S_l	ΔS_v	S_g
280.15	4.799 75	10.2901	5.0709	20 395.8	2524.2	22 920.0	20 862.3	3004.2	23 866.5	159.291	10.724	170.015
280.35	4.821 24	10.1998	5.1530	20 442.4	2436.1	22 878.5	20 915.1	2899.0	23 814.1	159.472	10.341	169.813
280.55	4.842 83	10.1037	5.2408	20 491.6	2342.3	22 833.9	20 970.9	2787.1	23 758.0	159.664	9.935	169.599
280.75	4.864 51	10.0007	5.3354	20 543.5	2242.1	22 785.6	21 029.9	2667.4	23 697.3	159.867	9.501	169.368
280.95	4.886 30	9.8894	5.4385	20 598.7	2134.0	22 732.7	21 092.8	2538.4	23 631.2	160.084	9.035	169.110
281.15	4.908 19	9.7677	5.5520	20 656.4	2016.1	22 672.5	21 158.9	2397.6	23 556.5	160.312	8.528	168.840
281.25	4.919 17	9.7020	5.6136	20 688.1	1952.5	22 640.6	21 195.1	2321.8	23 516.9	160.437	8.255	168.692
281.35	4.930 18	9.6324	5.6790	20 721.4	1885.4	22 606.8	21 233.3	2241.7	23 475.0	160.568	7.968	168.536
281.45	4.941 22	9.5583	5.7489	20 756.6	1814.0	22 570.6	21 273.6	2156.5	23 430.1	160.708	7.662	168.370
281.55	4.952 29	9.4788	5.8243	20 794.0	1737.4	22 531.4	21 316.5	2065.2	23 381.7	160.856	7.336	168.192
281.65	4.963 38	9.3928	5.9062	20 834.1	1654.7	22 488.8	21 362.5	1966.7	23 329.2	161.016	6.982	167.998
281.75	4.974 51	9.2986	5.9963	20 874.9	1564.5	22 439.4	21 409.9	1859.1	23 269.0	161.180	6.598	167.778
281.85	4.985 66	9.1938	6.0967	20 922.6	1464.2	22 386.8	21 764.9	1739.7	23 204.6	161.371	6.172	167.543
281.95	4.996 85	9.0747	6.2119	20 976.2	1352.4	22 328.6	21 526.8	1604.4	23 131.2	161.586	5.691	167.277
282.05	5.008 07	8.9346	6.3478	21 038.5	1217.4	22 255.9	21 599.0	1445.9	23 044.9	161.838	5.126	166.964
282.15	5.019 33	8.7604	6.5179	21 114.3	1052.4	22 166.7	21 637.3	1249.5	22 936.8	162.146	4.429	166.575
282.25	5.030 63	8.5154	6.7587	21 220.0	821.6	22 041.6	21 810.8	975.1	22 785.9	162.580	3.454	166.034
282.35	5.041 95	7.635	7.635	21 616.2	0.0	21 616.2	22 276.6	0.0	22 276.6	164.225	0.000	164.225

MPa, and $\rho_c = 7.6340 \pm 0.0009$ mol/dm^3.

Saturation Envelope

The only precise density data within the present critical region (280.15–284.15 K; 4.5–11.0 mol/dm^3) at the time were those of Douslin and Harrison (*1*) although later the measurements of Hastings and Levelt Sengers (*6*) were published. The latter measurements were not available at the start of this correlation and were not used in the correlation but only in comparison.

The orthobaric densities, ρ_l and ρ_g, were correlated via a combination of the law of rectilinear diameters and the power-law behavior of the coexisting density difference:

$$\bar{\rho}_{\sigma R} \equiv (\rho_l + \rho_g)/2\rho_c = 1 + k_1\tau_\sigma \qquad \tau_\sigma \equiv (T_c - T_\sigma)/T_c \quad (2)$$

$$(\Delta\rho)_{\sigma R} \equiv (\rho_l - \rho_g)/\rho_c = 2k_2\tau_\sigma^{\beta} \quad (3)$$

The maximum deviation of 11 experimental points of Douslin and Harrison from eq 2 is 3×10^{-3} mol/dm^3. Likewise, eq 3 fits the experimental values of $\Delta\rho$ within 5×10^{-3} mol/dm^3. Weighted least-squares values of the parameters are $k_1 = 0.7649 \pm 0.0014$, $k_2 = 1.8902 \pm 0.0146$, and $\beta = 0.3523 \pm 0.0084$, where the uncertainties equal twice the respective standard deviations. The critical exponent β agrees with the value of 0.35 of Douslin and Harrison (*1*). Several attempts to add higher ordered exponential terms to eq 3 resulted in statistical elimination. Also, temperature ranging (i.e., changing the lower temperature of the range T to T_c) does not affect significantly β: the range 258.15–CP yields the β above which changes only 0.7% when the range is increased to 238.16–CP. Equations 2 and 3 provide orthobaric densities from the CP to 258.15 K within the precision of the measurements. The densities of Angus et al. (*4*) have been shown by Nehzat (*7*) to deviate significantly from the law of rectilinear diameters and, understandably, from the later measurements of Douslin and Harrison (*1*).

Vapor Pressure

The nonanalytical vapor pressure equation of Walton et al. (*8*)

$$P_{\sigma R} \equiv P_\sigma/P_c = 1 - \Psi_c\tau_\sigma + k_7\tau_\sigma^{(2-\theta)} + k_8\tau_\sigma^{(2-\theta+\eta)} \quad (4)$$

correlates the measurements of Douslin and Harrison to better than 9 ppm from 258 K to the CP with the following parameters: $\theta = 0.2082 \pm 0.0012$, $\eta = 1.5476 \pm 0.4284$, $\Psi_c = 6.3696 \pm 0.0044$, $k_7 = 9.5355 \pm 0.0232$, and $k_8 = -6.4275 \pm 1.4246$. (Some constants are reported to more significant figures than justified by the accompanying uncertainty; the sole purpose of this practice is to allow precise reproduction of our tables with our equations and constants.) Deviations of the vapor pressure measurements of Hastings and Levelt Sengers (*6*) from eq 4 are less than 170 ppm over the same temperature range.

Enthalpy and Entropy of Vaporization

Combination of eq 2–4 with the Clapeyron equation provides

$$-(\Delta H_v)_R = 2Z_c k_2(1 - \tau_\sigma)\tau_\sigma^{\beta}[-\Psi_c + k_7(2 - \theta)\tau_\sigma^{1-\theta} + k_8(2 - \theta + \eta)^{1-\theta+\eta}][(1 + k_1\tau_\sigma)^2 - k_1^2\tau_\sigma^{2\beta}]^{-1} \quad (5)$$

where $(\Delta H_v)_R \equiv \Delta H_v/RT_c$, $Z_c \equiv P_c/(\rho_c RT_c)$, and $(\Delta S_v)_R \equiv \Delta S_v/R = (\Delta H_v)_R(T_c/T)$. Values of ΔH_v and ΔS_v, which appear in Table I, agree closely with those calculated by Douslin and Harrison (*1*) with a maximum deviation of 0.3%. All energy functions and entropy are absolute quantities referenced to perfect ethylene crystal at 0 K as chosen by Harrison and Douslin (*2*). The value of enthalpy referred to the perfect-gas state at 298.15 K is found by subtracting 29 610 J/mol whereas the entropy difference is 219.226 J/(K mol). The perfect-gas values used by Harrison and Douslin (*2*) are identical with those of Angus et al. (*4*).

Equation of State (EOS)

The isochoric EOS

$$P_R \equiv P/P_c = P_{\sigma R} + \Psi_\sigma(\tau_\sigma - \tau) + (\Phi_\sigma/2)(\tau - \tau_\sigma)^2 \quad (6)$$

is a Taylor series expansion of $P_R(\tau,\rho_R)$ along a given isochore with terms higher than second order truncated. Here, σ indicates a saturation property, Ψ is the dimensionless isochoric slope at its origin—the vapor pressure curve—or $\Psi_\sigma \equiv -(\partial P_R/\partial\tau)_\rho|_\sigma$, and Φ_σ is the analogous curvature function or $\Phi_\sigma \equiv (\partial^2 P_R/\partial\tau^2)_\rho|_\sigma$. Previously (*9*), Ψ_σ was found to have the same functional form as ρ_σ or

$$\bar{\Psi}_\sigma \equiv (\Psi_l + \Psi_g)/2 = \Psi_c + k_5\tau_\sigma \quad (7)$$

$$\Delta\Psi_\sigma \equiv \Psi_l - \Psi_g = 2k_6\tau_\sigma^{\lambda} \quad (8)$$

where the critical exponent λ is $^1/_2$ from either classical or scaling theory. For ethylene, $\lambda = 0.5304 \pm 0.0062$, $k_5 = 69.4549 \pm 0.8224$, $k_6 = 34.9071 \pm 0.0294$, and $\Psi_c = 6.372 \pm 0.016$. Since the slope of the critical isochore from the homogeneous-phase side equals the vapor pressure slope at the CP, this value of Ψ_c should be compared for consistency with our previous vapor pressure slope of $\Psi_c = 6.3696 \pm 0.0044$ and also with the value of 6.356 derived from the vapor

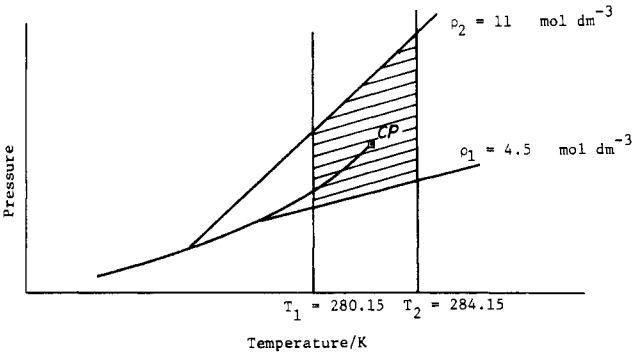

Figure 1. Present ethylene critical region.

pressure equation of Douslin and Harrison (*1*). Because of the low error band, the value of $\Psi_c = 6.3696$ was used for the remainder of this work. This slight adjustment of Ψ_c does not change significantly the above values of k_5, k_6, and λ.

The curvature function, Φ_σ, is well described by

$$\Phi_\sigma = \Phi_c(1 - \xi^4) + k_9(1 - \xi^2)\xi \exp(k_{10}\xi^2) \quad (9)$$

where $\xi \equiv (\rho_\sigma - \rho_c)/\rho_c$, $\Phi_c = 11.1017 \pm 0.6368$ (the curvature of the critical isochore at the CP), $k_9 = 282.9170 \pm 3.4278$, and $k_{10} = -10.4318 \pm 0.9312$.

Equation 6, together with eq 7–9, contains 13 constants and 3 critical exponents, i.e., k_1, k_2, k_5–k_{10}, Ψ_c, Φ_c, P_c, T_c, ρ_c, β, λ, and θ. The coexistence data, orthobaric densities, and vapor pressures provide k_1, k_2, k_7, k_8, Ψ_c, P_c, T_c, ρ_c, β, and θ. The remaining six parameters are determined from the homogeneous-phase densities. The present EOS, which represents the measured pressures of Douslin and Harrison (*1*) to better than 0.01% (*10*), should not be used far away from the critical region because the isochores have constant curvature. Further details concerning this EOS are found in ref *10*.

Entropy and Energy Functions

Ethylene energy functions and entropy were calculated in the homogenous-phase region of Figure 1 with $\rho_1 = 4.5$ mol/dm^3 as the base isochore. The isothermal variation of the entropy, S, and the Gibbs function, G, from the values of Harrison and Douslin (*2*) along ρ_1 were found by the identities

$$S_\rho - S_{\rho_1} = \int_\rho^{\rho_1} (\partial P/\partial T)_\rho (d\rho/\rho^2) \quad (10)$$

$$G - G_1 = \int_\rho^{\rho_1} (\partial P/\partial \rho)_T (d\rho/\rho) \quad (11)$$

The integrands were determined from the EOS and were integrated numerically. Values of the two derivatives were found by direct differentiation of eq 6:

$$(\partial P/\partial T)_\rho = (P_c/T_c)[\Psi_\sigma + \Phi_\sigma(\tau_\sigma - \tau)] \quad (12)$$

$$(\partial P/\partial \rho)_T = (P_c/\rho_c)\{[(dP_{\sigma R}/d\tau_\sigma) + \Psi_\sigma + (\tau_\sigma - \tau) \times (\Phi_\sigma + d\Psi_\sigma/d\tau_\sigma)](d\rho_{\sigma R}/d\tau_\sigma)^{-1} + (\tau - \tau_\sigma)^2(d\Phi_\sigma/d\xi)/2\} \quad (13)$$

A practical problem arises in evaluation of these derivatives—the same problem that occurs in finding $P(\rho,T)$ from eq 6. For given values of T and ρ, $T_\sigma(\rho)$ must first be found by inversion of

$$\rho_{\sigma R} = 1 + k_1\tau_\sigma \mp k_2\tau_\sigma^\beta \quad (14)$$

a combination of eq 2 and 3 with the upper sign denoting vapor and the lower sign liquid. In general, this inversion can only be performed numerically. Once T_σ (or τ_σ) is known from ρ, evaluation of P, $(\partial P/\partial T)_\rho$, and $(\partial P/\partial \rho)_T$ follows in a straightforward fashion from the previous equations.

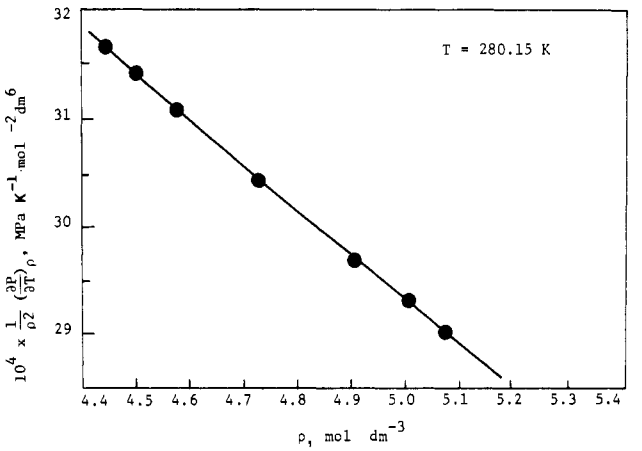

Figure 2. Integrand for entropy calculation, eq 10, at 280.15 K in the vapor state.

Table II. Homogeneous-Phase Thermophysical Properties of Ethylene along the Critical Isotherm (T = 282.35 K)

ρ, mol/dm^3	P, MPa	H, J/mol	G, J/mol	S, J/(mol K)
4.5000	4.8695	24 483	24 126	172.16
4.7234	4.9139	24 298	24 117	171.47
5.0000	4.9566	24 073	24 108	170.64
5.0709	4.9656	24 017	24 106	170.44
5.5000	5.0062	23 683	24 098	169.23
5.5520	5.0097	23 644	24 098	169.09
5.9062	5.0271	23 381	24 095	168.14
6.0000	5.0303	23 313	24 094	167.90
6.5000	5.0393	22 966	24 093	166.67
6.5179	5.0398	22 954	24 093	166.62
7.0000	5.0418	22 645	24 092	165.53
7.5000	5.0419	22.351	24 092	164.49
7.6349	5.0420	22 276	24 092	164.22
7.6351	5.0420	22 276	24 092	164.22
8.0000	5.0420	22 081	24 092	163.53
8.5000	5.0429	21 832	24 092	162.65
8.7604	5.0449	21 708	24 092	162.21
9.0000	5.0489	21 595	24 091	161.81
9.3928	5.0639	21 414	24 090	161.16
9.5000	5.0705	21 365	24 089	160.99
9.7677	5.0942	21 244	24 088	160.55
10.0000	5.1252	21 139	24 084	160.16
10.2901	5.1817	21 009	24 078	159.68
10.5000	5.2383	20 916	24 073	159.33
10.6790	5.2993	20 837	24 067	159.03
10.9991	5.4434	20 697	24 053	158.49
11.0000	5.4439	20 696	24 053	158.49

Figures 2 and 3 show the integrands in eq 10 and 11, respectively, for 280.15 and 283.15 K, respectively, to illustrate smoothness. Homogeneous-phase tables of density, pressure, enthalpy, Gibbs function, and entropy for isotherms from 280.15 to 284.15 K at 0.2 K intervals (21 isotherms) are available as supplementary material. (See paragraph at end of text regarding supplementary material.) The densities range from 4.5 to 11.0 mol/dm^3 at 0.5 mol/dm^3 intervals with 12 additional isochores. Table II, for the critical isotherm, is a sample of one such table. These tables supplement the wide-ranged tables (308.15–448.15 K, 0–16 mol/dm^3, and 0–40 MPa) of Harrison and Douslin (*2*) which provide the isotherms 280.15, 281.15, 282.15, 282.25, 282.35, and 283.15 in the present critical region (Figure 1). The present 26 isochores compare with a minimum of 11 (280.15 K) to a maximum of 22 (282.15 K) isochores for Harrison and Douslin.

Isochoric Heat Capacities

The entropies were numerically differentiated along isochores to determine the isochoric heat capacity, C_v. Calculated values are listed in Table III. A jump occurs in C_v in going from the homogeneous- to heterogeneous-phase region. At the CP itself,

Table III. Ethylene Isochoric Heat Capacities, C_v/(J/(mol K))

	ρ/(mol/dm^3) (T(sat.)/K)								
T/K	4.50 (278.363)	5.0 (279.966)	6.0 (281.754)	7.0 (282.310)	7.635 (282.35)[a]	8.0 (282.342)	9.0 (282.004)	10.0 (280.751)	11.0 (278.146)
280.15	50.4	53.7	166.5	151.0	143.1	139.3	130.1	122.8	46.2
280.25	50.3	53.6	167.2	151.8	143.6	139.8	130.6	122.9	46.1
280.35	50.2	53.6	168.5	152.5	144.0	140.5	131.2	123.3	46.0
280.45	50.2	53.5	169.3	153.1	144.9	141.1	131.8	124.1	46.0
280.55	50.1	53.4	170.1	154.0	146.0	141.8	132.6	125.2	45.9
280.65	50.0	53.4	171.4	155.0	146.4	142.6	133.2	126.0	45.8
280.75	50.0	53.3	172.6	156.0	147.8	143.6	134.0	126.6	45.8
280.85	49.9	53.2	174.0	157.1	148.3	144.5	134.7	51.3	45.7
280.95	49.8	53.2	175.5	158.5	149.9	145.6	135.5	51.2	45.6
281.05	49.7	53.1	177.1	160.0	151.0	146.7	136.6	51.2	45.6
281.15	49.7	53.1	178.8	161.4	152.6	148.2	137.8	51.1	45.5
281.25	49.6	53.0	181.0	162.8	153.8	149.7	139.0	51.0	45.4
281.35	49.5	52.9	182.8	164.2	155.8	151.2	140.6	51.0	45.4
281.45	49.5	52.9	185.0	166.9	157.0	153.2	142.4	50.9	45.3
281.55	49.4	52.8	187.5	169.1	160.0	155.3	144.5	50.9	45.3
281.65	49.3	52.7	189.9	171.7	162.1	156.5	146.2	50.8	45.2
281.75	49.3	52.7	196.6	174.2	164.7	159.8	148.6	50.8	45.1
281.85	49.2	52.6	62.7	179.0	169.5	163.0	152.8	50.7	45.1
281.95	49.1	52.5	62.6	185.0	174.1	168.5	157.5	50.6	45.0
282.05	49.0	52.5	62.6	192.2	180.0	174.0	57.9	50.6	44.9
282.15	49.0	52.4	62.5	200.9	187.7	181.2	57.8	50.5	44.9
282.25	48.9	52.3	62.5	217.2	202.3	195.0	57.8	50.5	44.8
282.35	48.8	52.3	62.4	74.9	∞/115.0	67.6	57.7	50.4	44.7
282.45	48.8	52.2	62.4	69.7	97.4	67.5	57.7	50.3	44.7
282.55	48.7	52.1	62.3	69.6	90.0	67.5	57.6	50.3	44.6
282.65	48.6	52.1	62.2	69.6	86.3	67.4	57.6	50.2	44.6
282.75	48.6	52.0	62.2	69.5	83.2	67.4	57.5	50.2	44.5
282.85	48.5	51.9	62.1	69.5	80.0	67.3	57.5	50.1	44.4
282.95	48.4	51.9	62.1	69.5	78.8	67.3	57.4	50.0	44.4
283.05	48.3	51.8	62.0	69.4	77.4	67.2	57.4	50.0	44.3
283.15	48.3	51.8	62.0	69.4	76.1	67.2	57.3	49.9	44.2
283.25	48.2	51.7	61.9	69.3	75.0	67.2	57.2	49.8	44.2
283.35	48.1	51.6	61.9	69.3	74.4	67.1	57.2	49.8	44.1
283.45	48.1	51.6	61.8	69.2	73.5	67.1	57.1	49.7	44.0
283.55	48.0	51.5	61.8	69.2	72.7	67.0	57.1	49.7	44.0
283.65	47.9	51.4	61.7	69.1	71.9	67.0	57.0	49.6	43.9
283.75	47.9	51.4	61.7	69.1	71.1	66.9	57.0	49.5	43.8
283.85	47.8	51.3	61.6	69.1	70.5	66.9	56.9	49.5	43.8
283.95	47.7	51.2	61.6	69.0	70.0	66.8	56.9	49.4	43.7
284.05	47.6	51.2	61.5	69.0	69.5	66.8	56.8	49.4	43.6
284.15	47.6	51.1	61.4	68.9	69.0	66.8	56.7	49.3	43.6

[a] Values of $(C_v)_{\rho_c}$ in this column.

C_v diverges from the two-phase side but is finite from the single-phase side. The latter feature is thermodynamically consistent with our finite value of Φ_c but does not agree with the basic scaling hypothesis which requires divergence from both sides along the critical isochore. In the two-phase region the divergence of C_v along the rectilinear diameter line is

$$(C_{v2,\rho})_R = k_3\tau^{-\alpha^*} \quad (15)$$

where $(C_v)_R \equiv C_v/R$, $k_3 = 11.1715 \pm 0.0692$, and $\alpha^* = 0.10106 \pm 0.02420$. Our C_v jumps, ΔC_v, are consistent with the identity

$$\Delta C_v = T_\sigma\rho_\sigma^{-2}(d\rho_\sigma/dT)[(dP_\sigma/dT) - (\partial P/\partial T)_\rho] \quad (16)$$

and eq 4, 6, and 14. The Yang–Yang identity (*11*)

$$C_v = (T/\rho)(\partial^2 P/\partial T^2)_\rho - T(\partial^2 G/\partial T^2)_\rho \quad (17)$$

provides a secondary consistency check for C_v values in the two-phase region, C_{v2}. Equation 17 demands (1) linearity for graphs of C_{v2} vs. specific volume (ρ^{-1}) along isotherms with $T(d^2P_\sigma/dT^2)$ as the slope and (2) linearity for graphs of ρC_{v2} vs. ρ along isotherms with $-T(d^2G_\sigma/dT^2)$ as the slope. The divergence of d^2P/dT^2 with exponent θ differs from that of C_{v2} with exponent α^* so that d^2G_σ/dT^2 is not analytic unlike scaled equations (*12*). Table IV presents the results of these graphs for ethylene with the value of $d^2P_{\sigma R}/d\tau^2$ compared to that calculated directly from the vapor pressure equation (eq 4).

Table IV. Ethylene $d^2G_{\sigma R}{}^a/d\tau^2$ and $d^2P_{\sigma R}/d\tau^2$ Values in the Critical Region

	$d^2P_{\sigma R}/d\tau^2$		$-d^2G_{\sigma R}/d\tau^2$
T_{68}/K	from eq 4	from C_v–ρ^{-1} graph	from ρC_v–ρ graph
281.35	43.8	42.3	7.35
281.55	45.9	44.1	7.27
281.75	48.7	47.0	7.17
281.95	53.0	52.3	6.90
282.25	70.7	69.4	5.04

[a] $G_{\sigma R} = G/RT_c$.

Finally, Table V provides thermophysical properties along the saturation envelope not found in Table I such as C_v and the sonic velocity, W_s. Equation 15 provides C_{v2}—within a unit J/(mol K) of the preferred values of Table V for temperatures above 281.55 K.

Accuracy of Tabular Values

All densities should be accurate to 0.05% considering the experimental data are judged better than 0.04%. The changes upon vaporization of the enthalpies, entropies, and internal energies of Table I have an estimated accuracy of 0.11%. In the single-phase region of Table II, the residual enthalpies,

Table V. Thermophysical Properties of Ethylene along the Coexistence Curve

T_{68}, K	$-dP_{\sigma R}/d\tau$	$d^2P_{\sigma R}/d\tau^2$	$C_{v2\bar{\rho}}$[a]	C_{v1l}[a]	C_{v2l}[a]	C_{v1g}[a]	C_{v2g}[a]	W_{s1l}[b]	W_{s1g}[b]
280.15	6.0041	37.10	146.8	50.6	125.1	54.2	190.9	258	201
280.35	6.0306	37.85	148.8	51.3	127.1	54.7	191.6	252	199
280.55	6.0577	38.70	150.9	52.0	129.3	55.3	192.4	247	198
280.75	6.0855	39.67	153.3	52.8	131.8	56.0	193.4	241	196
280.95	6.1139	40.80	156.2	53.9	134.9	57.1	194.9	235	194
281.15	6.1433	42.14	159.1	54.8	138.0	58.0	196.3	228	191
281.25	6.1584	42.91	160.8	55.3	139.8	58.5	197.1	225	190
281.35	6.1737	43.78	162.7	55.9	141.8	59.1	198.1	219	188
281.45	6.1894	44.75	164.8	56.6	144.1	59.8	199.3	215	187
281.55	6.2054	45.86	167.0	57.1	146.4	60.5	200.5	210	185
281.65	6.2291	47.16	169.8	58.0	149.4	61.5	202.2	205	183
281.75	6.2389	48.70	173.0	59.0	152.8	62.7	204.2	200	181
281.85	6.2564	50.59	176.6	60.0	156.7	63.9	206.6	195	178
281.95	6.2748	52.99	181.0	61.1	161.5	65.3	209.5	189	175
282.05	6.2941	56.27	186.4	62.1	167.3	66.7	213.1	181	171
282.15	6.3148	61.23	194.2	63.6	175.9	68.6	218.8	173	165
282.25	6.3380	70.70	207.3	65.3	190.3	71.5	228.8	159	156
282.35	6.3696	∞	∞	115.0	∞	115.0	∞	139	139

[a] Units: J/(mol K). [b] Units: m/s.

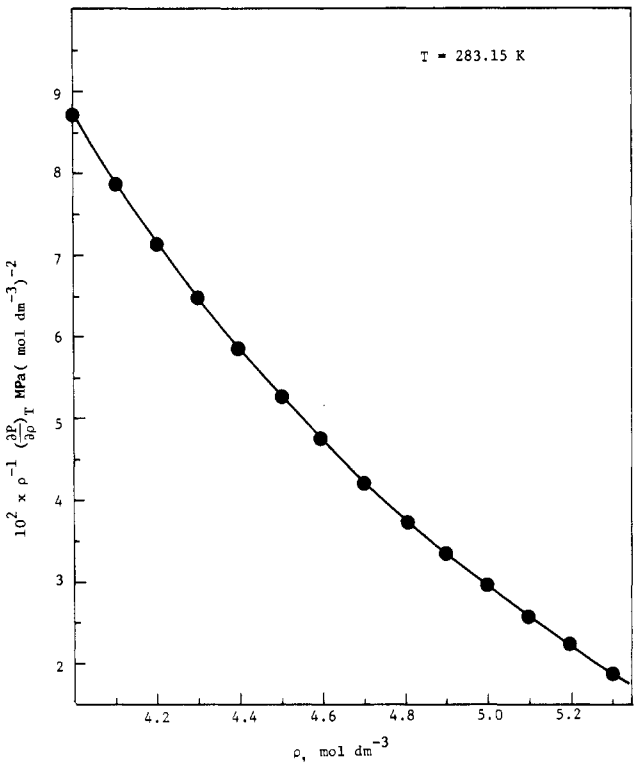

Figure 3. Integrand for Gibbs energy calculation, eq 11, at 283.15 K for the lower density range.

entropies, and Gibbs energies are judged accurate to 0.5% considering that the original density measurements have been differentiated once. A residual property is the value in the perfect-gas state less that of the real fluid all at the same pressure and temperature. Perfect-gas-state values are given by Harrison and Douslin (*2*).

The heat capacities of Tables III and V, which require a second differentiation, are considered accurate to 5%. Since the vapor pressure equation is considered accurate to 0.01%, values of the first and second derivatives of Table V should be valid to 0.1% and 1%, respectively. The sonic velocities of Table V should be accurate to ±5 ms^{-1}.

Finally, Table VI is a summary of all the constants used in the present correlation for the convenience of the reader.

Glossary

a_1–a_3	constants, eq 1
C_v	isochoric heat capacity, J/(mol K)

Table VI. Ethylene Parameters and Standard Deviations

parameter	value	SD
T_c, K	282.3502	0.0005
P_c, MPa	5.04197	0.00014
ρ_c, mol/dm^3	7.635	0.001
Z_c	0.2839	0.0032
α^*	0.10106	0.01210
β	0.3523	0.0042
λ	0.5304	0.0031
θ	0.2082	0.0006
η	1.5476	0.2142
Ψ_c	6.3696	0.0022
Φ_c	11.1017	0.3184
$(S_c)_R$	19.7507	0.0081
$(H_c)_R$	9.4893	0.0043
k_1	0.7649	0.0007
k_2	1.8902	0.0073
k_3	11.1715	0.0346
k_4	3.6711	0.0141
k_5	69.4549	0.4112
k_6	34.9071	0.0147
k_7	9.5355	0.0116
k_8	−6.4275	0.7123
k_9	282.9170	1.7139
k_{10}	−10.4318	0.4656

G	Gibbs energy, J/mol
H	enthalpy, J/mol
k_1–k_{10}	dimensionless constants ($k_4 \equiv Z_c\Psi_c k_2$)
P	pressure, MPa
R	gas constant, 8.314 33 J/(mol K) or dm^3 kPa/(mol K)
S	entropy, J/(mol K)
T	temperature, K (IPTS 68)
U	internal energy, J/mol
W_s	sonic velocity, m/s
Z_c	critical compressibility factor, $P_c/(R\rho_c T_c)$

Greek Letters

α	critical exponent for divergence of C_{v2}
β	critical exponent for saturation densities
η	second-order critical exponent of vapor pressure
θ	first-order critical exponent of vapor pressure
λ	critical exponent for isochoric slopes, $(\partial P/\partial T)_\rho\|_\sigma$
ξ	dimensionless density, $(\rho - \rho_c)/\rho_c$
ρ	density, mol/dm^3
τ	dimensionless temperature, $(T_c - T)/T_c$
Φ	dimensionless second derivative of an isochore, $(\partial^2 P/\partial T^2)_\rho(T_c^2/P_c)$
Ψ	dimensionless first derivative of an isochore, $(\partial P/\partial T)_\rho(T_c/P_c)$

Subscripts

c	at CP
g	gaseous phase
l	liquid phase
R	reduced property
v	change upon vaporization
$\bar{\rho}$	rectilinear diameter line, $(\rho_l + \rho_g)/2$
σ	coexistence property
1	single-phase property
2	two-phase property

Registry No. Ethylene, 74-85-1.

Literature Cited

(1) Dousiin, D. R.; Harrison, R. H. *J. Chem. Thermodyn.* **1976**, *8*, 301.
(2) Harrison, R. H.; Dousiin, D. R. *J. Chem. Eng. Data* **1977**, *22*, 24.
(3) Moldover, M. R. *J. Chem. Phys.* **1974**, *61*, 1766.
(4) Angus, S.; Armstrong, B.; de Reuck, K. M. "Ethylene, 1972"; Butterworths: London, 1972.
(5) Hastings, J. R.; Levelt Senger, J. M. H.; Balfour, F. W. *J. Chem. Thermodyn.* **1980**, *12*, 1009.
(6) Hastings, J. H.; Levelt Sengers, J. M. H. "Proceedings of the 7th Symposium on Thermophysical Properties"; American Society of Mechanical Engineers: New York, 1977; p 794.
(7) Nehzat, M. S. Ph.D. Dissertation, Texas A&M University, College Station, TX, 1978.
(8) Walton, C. W.; Mullins, J. C.; Holste, J. C.; Hall, K. R.; Eubank, P. T. *AIChE J.* **1978**, *24*, 1000.
(9) Hall, K. R.; Eubank, P. T. *Ind. Eng. Chem. Fundam.* **1976**, *15*, 80.
(10) Nehzat, M. S.; Hall, K. R.; Eubank, P. T. "Equations of State in Engineering and Research"; American Chemical Society: Washington, DC, 1979; Chapter 6.
(11) Yang, C. N.; Yang, C. P. *Phys. Rev. Lett.* **1964**, *13*, 303.
(12) Hall, K. R.; Eubank, P. T. *Ind. Eng. Chem. Fundam.* **1976**, *15*, 323.

Received for review October 1, 1981. Revised manuscript received July 28, 1982. Accepted January 20, 1983. Financial support of this project was by the National Science Foundation (ENG 76-00692).

Supplementary Material Available: The complete Table II containing the complete thermophysical properties of ethylene for isotherms ranging from 280.15 to 284.15 K at 0.2 K intervals for densities from 4.5 to 11.0 g-mol/dm^3 (21 pages). Table II of the manuscript is a sample for a single isotherm—the critical isotherm. Ordering information is given on any current masthead page.

Three-Phase Liquid–Liquid–Vapor Equilibria in the Methane + *n*-Pentane + *n*-Octane, Methane + *n*-Hexane + *n*-Octane, and Methane + *n*-Hexane + Carbon Dioxide Systems

Robert C. Merrill, Jr., Kraemer D. Luks,† and James P. Kohn*

Department of Chemical Engineering, University of Notre Dame, Notre Dame, Indiana 46556

The phase behavior of three ternary systems (methane + *n*-pentane + *n*-octane, methane + *n*-hexane + *n*-octane, methane + carbon dioxide + *n*-hexane) are presented for their region of L_1–L_2–V immiscibility. Liquid-phase compositions and molar volume data are presented as a function of temperature and pressure for the three-phase immiscibility region. The boundaries of the immiscibility regions are detailed. The methane + *n*-pentane + *n*-octane immiscibility is bounded by a locus of K points (L_1–L_2 = V), LCST points (L_1 = L_2–V), and Q points (S–L_1–L_2–V). The methane + *n*-hexane + *n*-octane immiscibility is bounded by a locus of K points, LCST points, and Q points and the L_1–L_2–V locus of the methane + *n*-hexane binary system. The methane + carbon dioxide + *n*-hexane immiscibility is bounded by a locus of K points and LCST points and by the L_1–L_2–V locus of the methane + *n*-hexane binary system. The L_1–L_2–V locus of the methane + *n*-hexane binary system is also presented.

Introduction

We are midway through an extensive study of liquid–liquid–vapor phenomena in liquefied natural gas systems. Earlier papers by Hottovy et al. (*1*, *2*) reported the phase behavior of the system methane + *n*-octane with the addition of a heavier solvent species. These heavier solvent species included ethane, propane, *n*-butane, and carbon dioxide. Hottovy showed that the addition of these species could induce L_1–L_2–V behavior in systems in which such behavior is not normally observed.

The three-phase regions studied by Hottovy were bounded by loci of K points (L_1–L_2 = V), LCST points (L_1 = L_2–V), and Q points (S–L_1–L_2–V), with a tricritical point at the point where the K-point and LCST-point loci intersect. Creek et al. (*3*) describe tricritical phenomena in systems containing methane and higher paraffins.

This paper presents the results for three new ternary systems which exhibit a region of immiscibility. These systems are methane + *n*-pentane + *n*-octane, methane + *n*-hexane + *n*-octane, and methane + carbon dioxide + *n*-hexane. The data presented herein include the compositions for the two liquid phases, and their molar volumes. The compositions and molar volumes for the bounding loci are also presented. The systems containing *n*-hexane are of great interest, because the methane + *n*-hexane binary forms its own L_1–L_2–V immiscibility locus. Data for the binary are presented and compared with earlier work by Lin et al. (*4*).

Experimental Section

This study employed apparatus previously used by Kohn and co-workers in other cryogenic studies (*5*). Earlier writings (*1*, *6*) have detailed the experimental procedure for L_1–L_2–V studies. For brevity's sake, the procedure will be only quickly sketched here.

All the phenomena were observed in a glass cell marked and calibrated for visual inspection. Stoichiometric and volumetric measurements were used to compute the compositions and molar volumes of each phase. A platinum resistance thermometer was used to measure the temperature of the system. This thermometer was calibrated to the 1968 IPTS scale and

† Present address: Department of Chemical Engineering, University of Tulsa, Tulsa, OK 74104.

0021-9568/83/1728-0210$01.50/0